Structures Formed in Spin-Cast Films of Polystyrene Blends with Poly(butyl methacrylate) Isomers

J. Raczkowska,[†] A. Bernasik,[†,‡] A. Budkowski,[*,†] K. Sajewicz,[†] B. Penc,[†] J. Lekki,[§] M. Lekka,[§] J. Rysz,[†] K. Kowalski,[†,‡] and P. Czuba[†]

M. Smoluchowski Institute of Physics and Joint Center for Chemical Analysis and Structural Research, Jagellonian University, Reymonta 4, 30-059 Kraków, Poland; Faculty of Physics and Nuclear Techniques and Faculty of Metallurgy and Materials Science, AGH−University of Science and Technology, Mickiewicza 39, 30-059 Kraków, Poland; and Institute of Nuclear Physics, Polish Academy of Sciences, Radzikowskiego 152, 31-342 Kraków, Poland

Received December 2, 2003; Revised Manuscript Received June 28, 2004

ABSTRACT: For polystyrene blends with poly(butyl methacrylate), replacing poly(*n*-butyl methacrylate) by poly(*tert*-butyl methacrylate) results in modified topography of spin-cast films (holes dominating at a surface are exchanged with islands, or vice versa, such individual surface features are increased), decreased PBMA surface excess, but similar overall domain structure. Two series (PS/PnBMA and PS/PtBMA) of films with constant thickness and PBMA fraction $0 < \Phi < 1$, cast from toluene onto silicon wafers, were examined with atomic force microscopy, X-ray photoelectron spectroscopy, profiling and mapping mode of dynamic secondary ion mass spectrometry. Topography was analyzed with the integral geometry approach. Film structure formation was postulated to involve surface segregation, phase separation, and instability of the transient PBMA layer [a linear relation between Φ^2 and averaged size of holes (islands) was observed for PS/PnBMA (PS/PtBMA)]. Structural changes caused by isomer exchange are related to glass transition temperature and blend incompatibility; both increased for PtBMA.

1. Introduction

Polymer multiphase thin films with specific morphologies are of great technological importance.[1−6] Phase domain arrangement in thin films, reflected often by surface topography, is usually a result of phase separation process, qualitatively different from that in the bulk (for a review, see refs 7−12). In the past decade most of the fundamental investigations of polymer blend films have analyzed temperature-driven phase separation (and wetting) where well-defined one-step quench to a fixed point of the phase diagram is followed by quasi-static phase evolution.[7−10,12] In turn, the phase separation and related structure formation that occur in polymer blend films during spin-casting from a common solvent, although more relevant for the industry, have been studied only very recently.[4,10−32] The situation is here much more complex: Phase demixing, initiated along the quench path with solvent concentration varying with time and position within the film, is followed by non-quasi-static structure evolution competing with solvent evaporation and different hydrodynamic regimes of film fluid, leading often to long-lived metastable morphologies.[11,12,32−37]

Multiple mutually coupled mechanisms effective during spin-casting of polymer blend films are not completely resolved, but main factors critical for film structures formed have been recognized.[11,13−17,20,21,24,26,29−32] However, *microstructural mechanisms* of film structure formation, although intensively studied for temperature-quenched blends,[9,38−40] have been analyzed only sporadically for the mixtures quenched by solvent extraction (e.g., for slowly drying layers rather than spin-cast films[41]). Another currently discussed main issue is phase evolution in the cast films,[14,15,18−20,28−30,32,36,42] in particular the relevance of *interfacial (capillary) instability*[43−46] breaking up transient lamellar phase arrangement (advocated in refs 15, 18, 23, and 32 and tested for feature size scaling with total film thickness[19]). While practically all published data on spin-cast polymer blend films are analyzed only qualitatively (because of the complexity of the formed structures), the advent of integral geometry approach[47−51] (and equivalent simpler evaluations[19,20,24]) has allowed for a more *quantitative description* in the most recent reports.[19,29]

In this work, we study microstructural mechanisms of film structure formation in spin-cast films of polystyrene (PS) blends with poly(butyl methacrylate) (PBMA) isomers: poly(*n*-butyl methacrylate) (PnBMA) and poly(*tert*-butyl methacrylate) (PtBMA). Formed film morphologies, determined with microscopic (atomic force microsopy, AFM) and spectroscopic techniques (X-ray photoelectron spectroscopy, XPS, profiling and mapping mode of dynamic secondary ion mass spectrometry, dSIMS), are analyzed with the integral geometry approach. Morphological differences and similarities of two blend series (PS/PnBMA and PS/PtBMA) are used not only to elucidate microstructural aspects of film structure formation but also to relate all results within one formation model. The presented quantitative test for the compositional scaling of the size of individual dropletlike domains indicates that interfacial (capillary) instability can explain origins of morphologies observed in spin-cast films of both polymer blends.

2. Experimental Section

2.1. Preparation of Polymer Blend Films. Measurements are reported here for PS blends with two PBMA isomers, PnBMA and PtMBA. Physical properties of pure blend components[52−56] are listed in Table 1, and molecular

[†] Jagellonian University of Kraków, Poland.
[‡] AGH−University of Science and Technology, Kraków.
[§] Institute of Nuclear Physics, PAS, Kraków.
* Corresponding author: e-mail ufbudkow@cyf-kr.edu.pl; fax ++48-12-633 70 86; phone ++48-12--632 48 88.

10.1021/ma035815h CCC: $27.50
Published on Web 08/25/2004

Table 1. Physical Properties of Materials Used in This Study

	M_n	M_w/M_n	surface tension γ/mJ m^{-2}	glass transition T_g/K	solubility parameter δ/MPa$^{1/2}$
PtBMA	554K	1.11	30.4[a]	395[a]	17.7[b]
PnBMA	484K	1.07	31.2[a]	293[a]	17.8−18.4[c] (17.9[d])
toluene			28.5[e]		18.2[a]
PS	564K	1.03	40.7[a]	373[a]	17.5−18.7[a] (18.0[d])

[a] Reference 52. [b] Reference 53. [c] Reference 54. [d] Theoretical value.[55] [e] Reference 56.

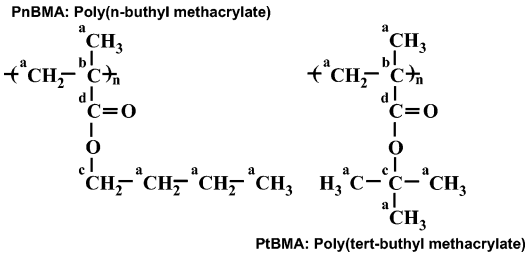

Figure 1. Molecular formulas of PnBMA and PtBMA.

structures of the isomers used are shown in Figure 1. Pure polymers were used to prepare two blend series PS/PnBMA and PS/PtBMA, each with PBMA weigh fraction Φ varying between 0 and 1. Blend films were prepared by spin-casting (5000 rpm for 40 s) from toluene solutions (constant total polymer concentration of 20 mg/mL was used) onto silicon wafers with native oxide (SiO_x) or with evaporated (∼50 nm thick) Au layer. Deuterated polystyrene (dPS, $M_w = 713$K, $M_w/M_n = 1.05$) was used as PS counterpart to provide contrast for dSIMS.

2.2. Characterization of Polymer Blend Films. Surface topography formed in the course of spin-casting was examined by AFM working in contact mode. Images were recorded in air at room temperature[29,59] with the home-built[57] AFM apparatus[59] and with CP Park Scientific Instruments AFM microscope.[29] Film thickness $\langle h \rangle$ was determined from AFM images taken after partial removal of the polymer film by a scalpel scratch.[28]

Surface chemical composition of blend (PS/PnBMA, PS/PtBMA) and reference polymer (PS, PnBMA, PtMBA) films, all cast on SiO_x, was evaluated on the basis of XPS spectra obtained with a Specs ESCA spectrometer with Mg Kα source working at 15 kV and 20 mA.[30] All C_{1s} peaks were charge referenced to the neutral carbon peak at the binding energy of 285.0 eV.[13,18,60]

Vertical and horizontal aspects of phase domain structure in the blend films were provided by depth profiling (depth resolution of ∼10 nm) and mapping (lateral resolution of ∼120 nm was achieved[61]) dSIMS modes, respectively.[61] The latter yielded lateral composition maps $\Phi_{PS}(x,y)$[12,27,29−31,61] corresponding to the distribution of PS counterpart (dPS) in the film. The former provided depth profiles[12,27,29−31,58,59,61] of the average composition. The dSIMS data were obtained with a VSW apparatus equipped with a high-resolution ion gun (liquid metal, Fei Co.) and a Balzers quadrupole mass spectrometer. A primary Ga^+ ion beam (5−25 keV, 0.2−4 nA) was used to sputter the sample and to induce secondary ions, which yielded mass-resolved information for the maps and the profiles.[61] The maps of dPS (C_2D^-, $m/z = 26$) as well as the profiles of Si (Si^-, $m/z = 28$) and all the polymers (C_2^-, $m/z = 24$) were provided by individual signals. To obtain a measure related to the fractional concentration of PBMA in a polymer film, original signal (C_2H^-, $m/z = 25$) was normalized by the $m/z = 24$ yield. Only single composition maps $\Phi_{PS}(x,y)$ were obtained for each analyzed film due to low yield of the secondary ions C_2D^- ($m/z = 26$).[30,61] Lateral resolution of the maps recorded for the dPS/PnBMA ($\Phi = 0.65$) and dPS/PtBMA ($\Phi = 0.70$) films (cast on Au) corresponds to ∼200 and ∼600 nm, respectively.

3. Results

3.1. Surface Topography. AFM Images. Representative surface morphologies, determined with AFM

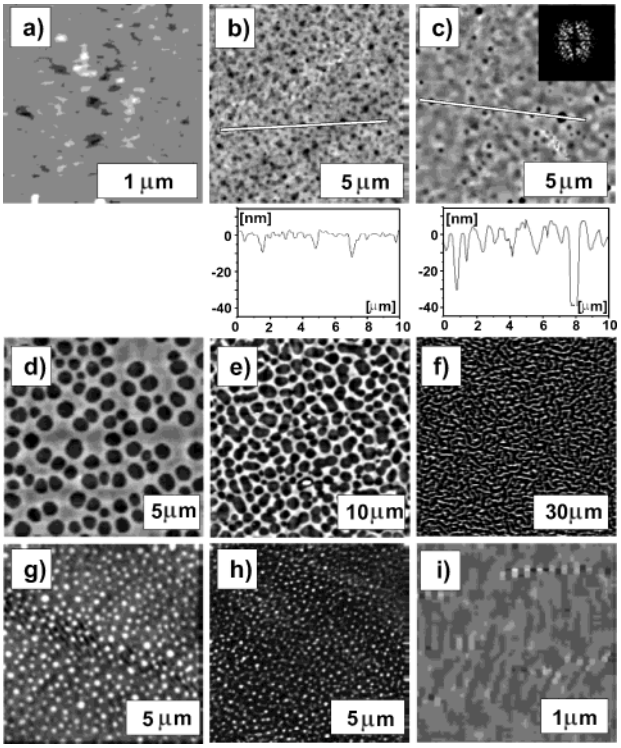

Figure 2. AFM images of free surface topography formed by PS/PnBMA films spin-cast on SiO_x substrate for PBMA mass fraction $\Phi = 0$ (a), 0.10 (b), 0.30 (c), 0.50 (d), 0.60 (e), 0.70 (f), 0.80 (g), 0.90 (h), and 1.0 (i). Different height ranges ΔH were applied to maximize the contrast. $\Delta H = 2$ (a), 16 (b), 40 (c), 42 (d), 66 (e), 34 (f), 21 (g), 10 (h), and 2 nm (i). The inset in the (c) represents the fast Fourier transform spectrum. The cross sections correspond to the lines in (b) and (c).

for PS/PnBMA and PS/PtBMA blend films cast on SiO_x substrate, are collected in Figures 2 and 3, respectively. Films of pure blend components (Figures 2a,i and 3a,i) are fairly featureless (note that statistical height fluctuations are visible only when height range $\Delta H = 2-4$ nm is used). In contrast, blending these polymers results in distinctive ($\Delta H = 10-66$ nm, see Figures 2b−h and 3b−h) and isotropic surface patterns (their fast Fourier transform spectra exhibit diffusive rings, see e.g., insets in Figures 2c and 3c). Surface morphologies evolve with increasing PBMA blend composition Φ. For the PS/PnBMA films (Figure 2b−h) hole-dominated topographies formed at low Φ evolve via elongated large-scale nearly bicontinuous structures (at $\Phi \sim 0.70$) into the patterns dominated (for higher Φ) by isolated protrusions. These surface patterns are strongly affected when PnBMA is replaced by PtBMA (cf. Figures 2b−h and 3b−h): Holes dominating at surface are exchanged with islands or vice versa for $\Phi < 0.70$ or $\Phi > 0.70$, respectively. In addition, individual dominant surface features (holes or islands) are larger for the PS/PtBMA films. Surface patterns, closely resembling those of Figures 2 and 3, are also formed by the PS/PBMA blend films cast onto gold substrate. We note also two ad-

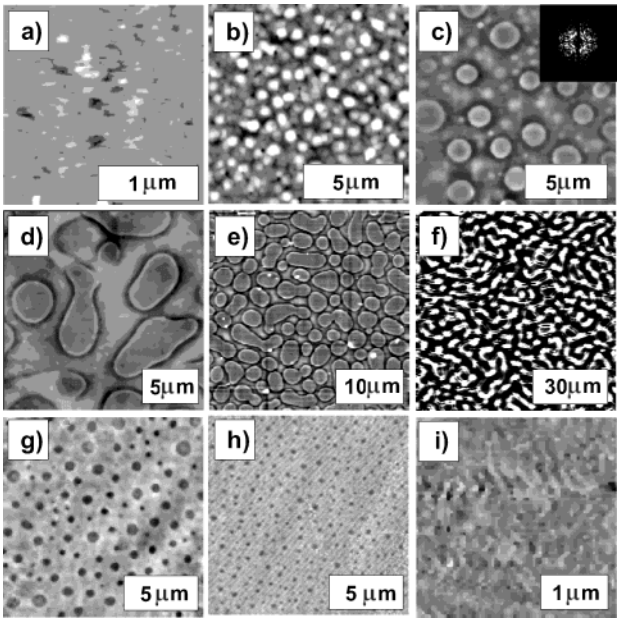

Figure 3. As Figure 2 but for PS/PtBMA films. Height ranges $\Delta H = 2$ (a), 10 (b), 11 (c), 34 (d), 31 (e), 31 (f), 13 (g), 11 (h), and 4 nm (i).

ditional properties of PS/PnBMA films: First, weak (with ~10 nm amplitude) film surface undulations, forming elongated ribbonlike structures, accompany deep (even of ~40 nm) holes recorded for the $\Phi = 0.30$ film (Figure 2c). A similar situation is exhibited by other blends with $\Phi \leq 0.40$ (e.g., Figure 2b). Second, the hole-dominated surface patterns are much less distinct[26] (or not resolved[24]) for much thinner films in this composition range. Both properties are expected for destabilization process[43,46] of transient solvent layer rich in one blend component (PBMA), postulated for the spin-casting process.[15,18,19,32] We will discuss this point in detail in section 4.

Analysis with Integral Geometry Approach. The topography data were analyzed with the integral geometry approach[47−51] as described in detail earlier.[29] Blend ($0.10 < \Phi < 0.90$) film surfaces exhibit bimodal height h-distribution (centered at $\langle h_1 \rangle$ and $\langle h_2 \rangle$). The surface pattern of each blend film is characterized by its vertical extent ($\Delta h = \langle h_2 \rangle - \langle h_1 \rangle$) and lateral morphological measures: the area fraction F (coverage) and the Euler characteristic χ_E (connectivity) of the elevated regions (i.e., with local height $h > (\langle h_2 \rangle + \langle h_1 \rangle)/2$).[62] χ_E is defined as the difference between the number of separated elevated and depressed regions. The vertical extent Δh values of PS/PnBMA films are higher than those determined for PS/PtMBA blends. For PS/PnBMA, Δh exhibits maximum of 60(12) nm at $\Phi \sim 0.60$ and decreases monotonically for larger and lower blend composition. In turn, the vertical extent for PS/PtBMA is nearly constant with Δh ~18(10) nm. These values can be compared with the thickness $\langle h \rangle$, constant for different blend compositions and similar for both film series, with the averaged values of 102(10) and 111(14) nm for PS/PnBMA and PS/PtBMA, respectively.

The integral geometry approach provides morphological measures for a series of surface patterns (the coverage F plotted in Figure 4a) and for individual (dominant) features of these patterns (Figure 4b). The dominant features correspond to holes (open symbols in Figure 4b) and islands (solid symbols) for negative and positive χ_E values, respectively. The individual

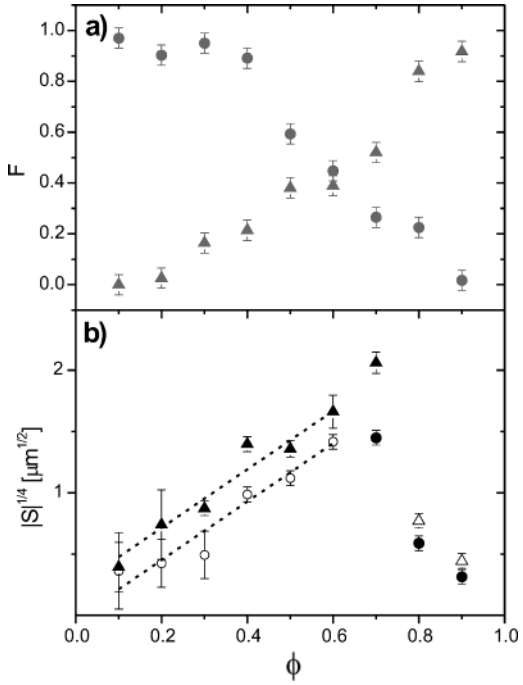

Figure 4. (a) Area fraction F of elevated surface regions and (b) fourth root $|S|^{1/4}$ of average area of individual dominant surface feature (hole, open symbols, or island, solid symbols) formed by the film blends PS/PnBMA (circles) and PS/PtBMA (triangles) with different composition Φ cast onto SiO_x. The trend $|S|^{1/4} \sim \Phi$, suggested by interfacial instability mechanism,[43,44] is marked (dotted lines) for comparison.

dominant surface feature is characterized by its average area $S = (1 - F)/\chi_E$ for $\chi_E < 0$ and $S = F/\chi_E$ for $\chi_E > 0$.[29] Figure 4b represents the compositional relation of fourth root of the average area $|S|^{1/4}$, used later (section 4) to discuss the mechanism of film structure formation. For PS/PtBMA series, the fractional area F of elevated surface regions (triangles in Figure 4a) increases monotonically with PBMA blend fraction, suggesting that surface elevations correspond to domains rich in PtBMA. Average area $|S|$ of islands increases with PtBMA composition Φ up to $\Phi_{i-h} = 0.75(4)$ (triangles in Figure 4b), when island-dominated almost bicontinuous structures are transformed into holes, decreasing in size $|S|^{1/2}$ for higher PtBMA content. For PS/PnBMA series, the surface coverage F of elevated regions decreases with blend PBMA composition (circles in Figure 4a). This decrease is very weak up to $\Phi = 0.40$ (with $F \geq 0.89$), but then F diminishes monotonically suggesting that surface depressions are related with PnBMA-rich domains (section 3.3). The hole-dominated surface patterns of the first composition region, with very low [$(1 - F) < 0.12$] surface coverage by holes, were not observed[24] or reported as much less distinct[26] for much thinner films. The lateral length scale of dominant surface features (see circles in Figure 4b) mimics the compositional dependence mentioned above for PS/PtBMA (triangles in Figure 4b), but its values are always smaller. Average area $|S|$ of holes increases with PBMA composition Φ up to $\Phi_{i-h} = 0.65(4)$ when hole-dominated almost bicontinuous structures are transformed into islands, decreasing in size $|S|^{1/2}$ for higher PnBMA content. We note also the same trend in the $|S|^{1/4}$ vs Φ relation for all hole-dominated surface morphologies in PS/PnBMA (open circles in Figure 4b). This suggests an identical mechanism responsible for hole formation (section 4), less effective for PBMA

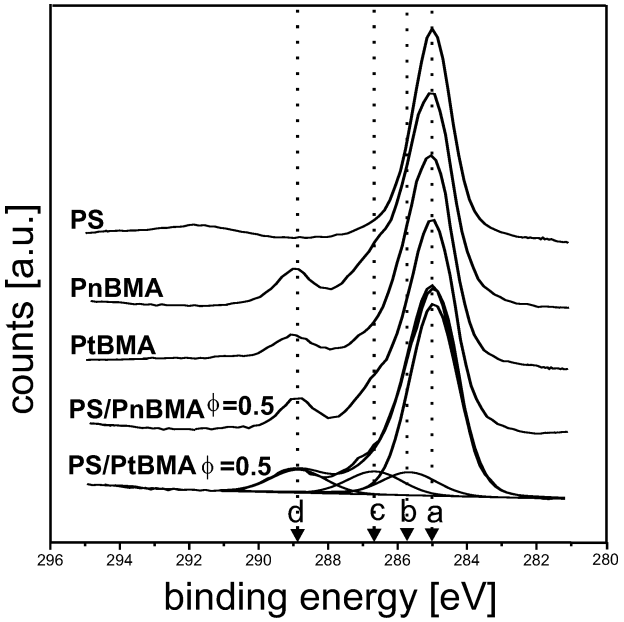

Figure 5. XPS C_{1s} core-level spectra of PS, PnBMA, PtBMA, and the $\Phi = 0.50$ blends: PS/PnBMA and PS/PtBMA; all films are positioned on SiO_x. Contributions to the C_{1s} envelope are shown for the last spectrum, and their positions are marked by dashed arrows and referred to various carbon environments[60] in PnBMA and PtBMA (cf. Figure 1).

composition $\Phi \leq 0.40$ (Figure 4a). The linear $|S|^{1/4}$ vs Φ relation determined for holes in PS/PnBMA seems to be reproduced (with larger $|S|$ values) by islands in PS/PtBMA.

3.2. Surface Composition. Figure 5 shows the XPS C_{1s} spectra determined for the symmetric ($\Phi = 0.50$) blend films PS/PnBMA and PS/PtBMA as well as for the reference homopolymer films of PS, PnBMA, and PtBMA, all positioned on SiO_x. The C_{1s} envelope of PnBMA and PtBMA can be resolved into four contributions (a−d) referred to neutral carbon ^{a}C at 285.0 eV and three carbons with different electron-deficient environments (represented in Figure 1): ^{b}C at 285.7 eV, ^{c}C at 286.7 eV, and ^{d}C at 288.9 eV.[24,60] PS exhibits a single peak coincident with ^{a}C and shake-up satellites of low intensity, centered at ca. 291.8 eV[60] and falling outside the C_{1s} envelope of PBMA. The XPS spectra determined for both blend film series were fitted with four peaks (a−d), assuming the binding energies given above and two independent intensities $I(^{a}C)$ and $I(^{d}C) = I(^{c}C) = I(^{b}C)$. The surface PBMA weight fraction Φ^S was calculated using the relation $I(^{d}C)/I_{total} = (\Phi^S/M_{BMA})/[(8\Phi^S/M_{BMA}) + (8(1 - \Phi^S)/M_{PS})]$.[13] I_{total} is the integrated intensity of the whole spectrum; M_{BMA} and M_{PS} are the molecular weights for butyl methacrylate and styrene monomer units, respectively.

The relation of surface Φ^S vs bulk Φ composition determined for films PS/PtBMA (triangles) and PS/PnBMA (circles) is presented in Figure 6. We observe that replacing PtBMA by PnBMA results in strongly increased PBMA surface excess (detected in ∼7 nm thick near-surface region sampled by XPS[30,60]). The surface PBMA composition Φ^S of PS/PtBMA blends scales almost linearly with (nominal) bulk concentration Φ, indicating very weak surface excess. In turn, the Φ^S vs Φ dependence of PS/PnBMA series shows strong PBMA segregation approaching saturation (with $\Phi^S \geq 0.93$) already for bulk compositions $\Phi > 0.60$. The latter result is in accord with earlier observations.[24,26] We note

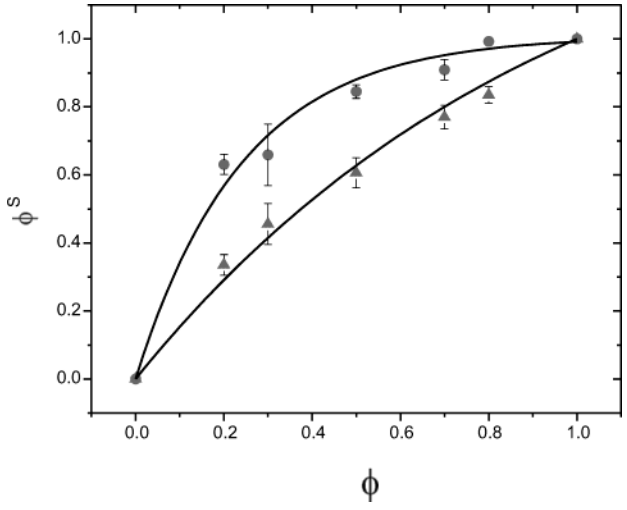

Figure 6. PBMA surface weight fraction Φ^S as a function of mixture composition Φ determined with XPS for blend films PS/PnBMA (circles) and PS/PtBMA (triangles) on SiO_x. Lines are a guide to the eye.

also the relation (section 4) between the surface excess and surface topography of spin-cast blend films. Less pronounced surface patterns (observed in PS/PnBMA with the $|S|$ values smaller than in PS/PtBMA, Figure 4b) correspond to stronger surface excess in blend component (PBMA) with lower surface tension γ.

3.3. Domain Structure. Vertical Film Structure. PS/PnBMA. To trace vertical extent of phase domains, the profiling dSIMS mode was used. Results obtained for PnBMA blends are exemplified by the data (Figure 7) corresponding to the dPS/PnBMA ($\Phi = 0.65$) film cast onto Au substrate. The profiles in Figure 7 exhibit three consecutive sputtering periods, best characterized by different regions of the carbon profile ($m/z = 24$, open triangles) on the logarithmic plot. We propose to relate these three sputtering periods with the following situations: First, a continuous undulated blend film with laterally arranged domains (see sketch I in Figure 7c) is present. Second, lateral PBMA-rich phase domains are sputtered away faster than those rich in PS (sketch II in Figure 7c), and therefore the PBMA fraction (open circles) in the blend layer left is decreased and Si wafer ($m/z = 28$, solid triangles) becomes partially exposed. Finally, all the polymer material (open triangles) is etched and the Si signal is saturated.

In addition to overall lateral phase domain structure, the PnBMA profile (open circles) indicates strong PBMA enrichment (see late times of the II-nd sputtering period) in the regions of PS-rich domains adjacent to the substrate (with PnBMA fraction in this fragmented layer higher than in the continuous blend film of regime I). PBMA excess at the free surface, suggested by a single data point, was confirmed by XPS results (section 3.2).

PS/PtBMA. Results obtained for PtBMA blends are represented by the data (Figure 8) corresponding to the dPS/PtBMA ($\Phi = 0.70$) film cast onto Au substrate. Recorded depth profiles resemble those characteristic for PnBMA films (cf. Figure 7). A similar overall lateral phase domain arrangement (sketch I in Figure 8) and sputtering scenario is concluded, but no distinct PBMA excess at the substrate is observed (a similar result was obtained by XPS for the free surface, section 3.2). Domains rich in PS (dPS) are now not elevated (as for PnBMA blends) but rather slightly lowered below the

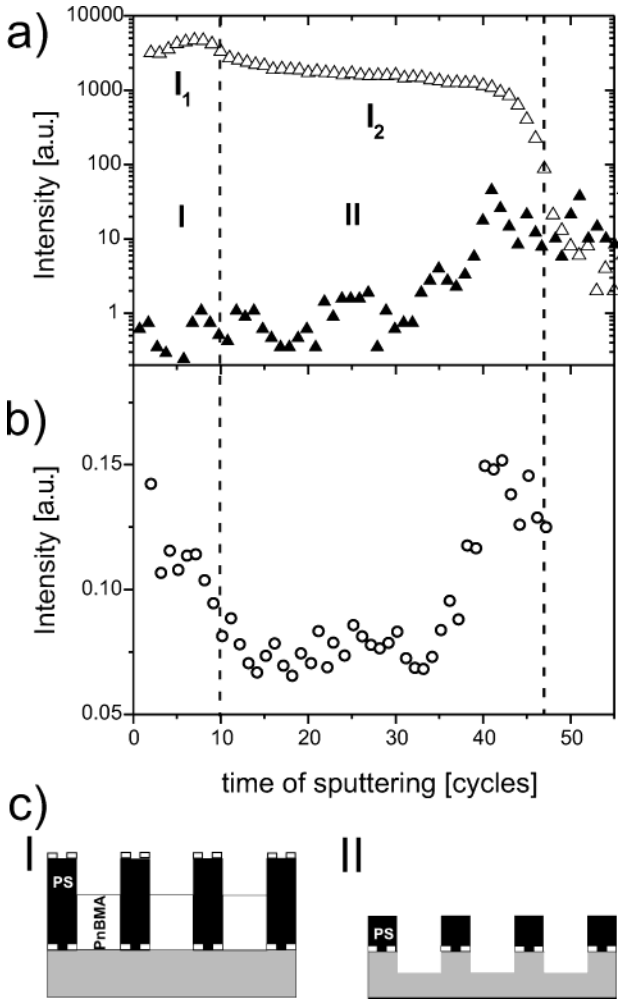

Figure 7. Overall phase arrangement in the dPS/PnBMA (Φ = 0.65) film on Au, as determined with profiling dSIMS mode. (a, b) Profiles corresponding to total polymer composition (m/z = 24, open triangles), Si concentration (m/z = 28, solid triangles), and the fraction of PnBMA (m/z = 25 normalized by m/z = 24, open circles) in the polymer film. Sputtering time measures the distance from original surface (1 cycle ∼2.7 and ∼8.3 nm for dPS and PnBMA, respectively). (c) Sketch to illustrate sectional view of (deuterated PS and PnBMA) phase domains exposed in consecutive sputtering periods. Layers enriched in PBMA, adjacent to surface and substrate, are marked by white (short) dashed lines.

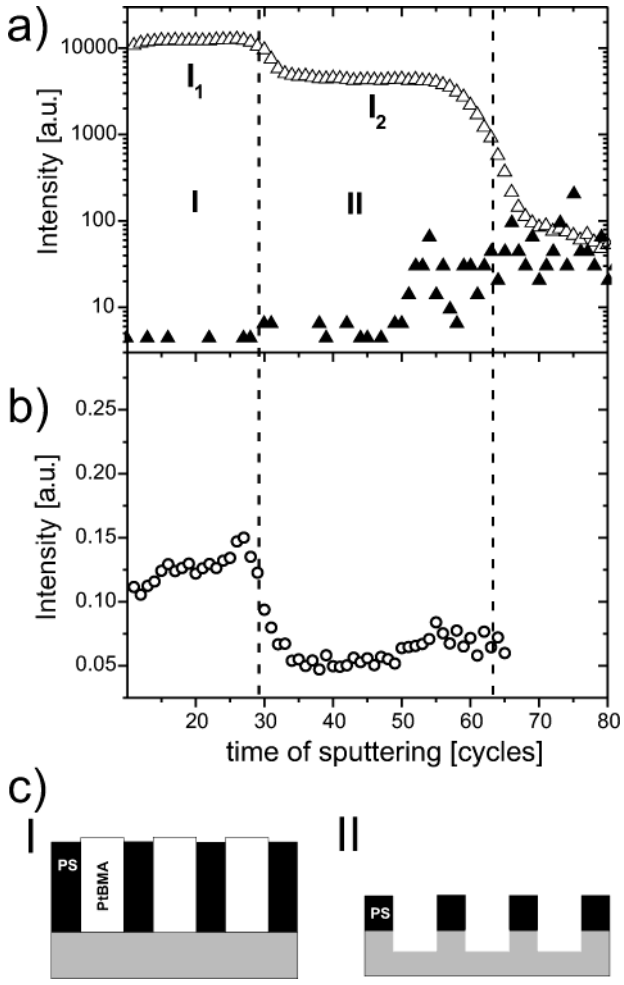

Figure 8. (a, c) As Figure 7 but for the dPS/PtBMA (Φ = 0.70) film on Au (1 cycle ∼1.6 and ∼4.0 nm for dPS and PtBMA, respectively). (b) Profile corresponding to the PtBMA fraction (m/z = 25 normalized by m/z = 24, open circles) in the polymer film.

level of PBMA domains. However, PS-rich lateral domains are again sputtered slower than PBMA regions (in accord with the data reported for PS and methacrylic polymers[63]).

Horizontal Film Structure. The overall lateral phase domain arrangement, indicated by the depth profiles obtained with dSIMS (sketch I in Figures 7c and 8c), was confirmed by the mapping mode of this technique.[61] Lateral distribution maps of polystyrene (dPS, Figure 9b,d), determined for dPS/PnBMA (Φ = 0.65) and dPS/PtBMA (Φ = 0.70) blend films, are compared with surface topography of the same samples examined with AFM (Figure 9, a and c, respectively). For the dPS/PnBMA mixture (Figure 9a,b), the continuous ribbon-like structures formed by the elevated domains correspond to film regions rich in polystyrene (cf. sketch I in Figure 7c), in accord with the results of photoemission electron microscopy.[24] For the dPS/PtBMA (Φ = 0.70) blend (Figure 9c,d), the wider elongated (sometimes circular) slightly higher domains correspond to film regions rich in PtBMA while the interconnected narrow ribbons of lower surface areas are formed by the polystyrene domains (cf. sketch I in Figure 8c). Such an interpretation is confirmed by the following observation: the surface fraction of elevated areas in Figure 9a, F = 0.42(4), and (slightly) lower domains in Figure 9c, $(1 - F)$ = 0.32(4), agree well with the ratio of m/z = 24 intensity averaged for two sputtering periods I_2/I_1 = 0.39(6) (Figure 7) and I_2/I_1 = 0.34(7) (Figure 8), respectively.

4. Discussion

Structure Formation in Spin-Cast Films. The data presented in the previous section will be now used to put forward a model of structure formation in spin-cast films of PS/PBMA blends, taking into account similarities and differences in physicochemical properties of PBMA isomers (Table 1). This scenario is based on the extension of earlier models.[11−15,18−20,22,28−32,34,35] The spin-casting consists of three consecutive stages. First, most of the polymer solution is spun off, leaving a uniform film (Figure 10a).[34] Second, radial flow of the fluid, which is a balance between centrifugal and viscous forces, decreases film thickness and controls its final average value.[28,31,34,35,64] It is during this stage that phase separation occurs for immiscible blends (Figure 10b−d), initiated by decreasing solvent concentration

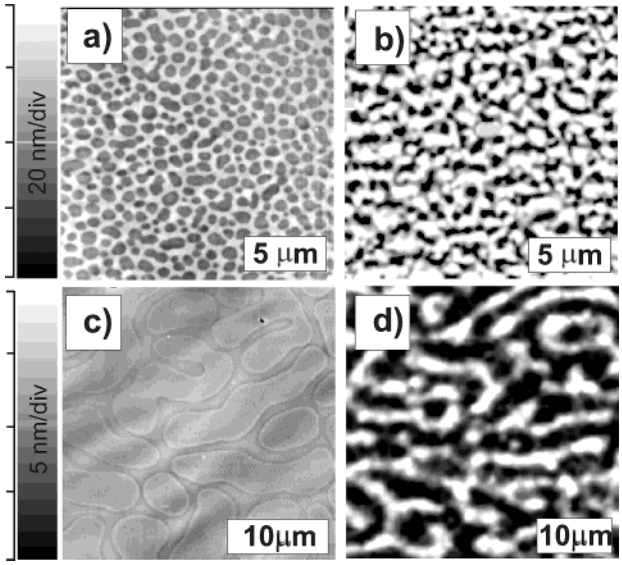

Figure 9. Surface topography (a, c) and lateral distribution maps of polystyrene dPS (b, d) determined with AFM and mapping dSIMS mode, respectively, for the dPS/PnBMA ($\Phi = 0.65$) film on Au (a, b; cf. Figure 7) and dPS/PtBMA ($\Phi = 0.70$) film on Au (c, d; cf. Figure 8). The gray scale depicts height or composition scale (black and white correspond to low and high values, respectively).

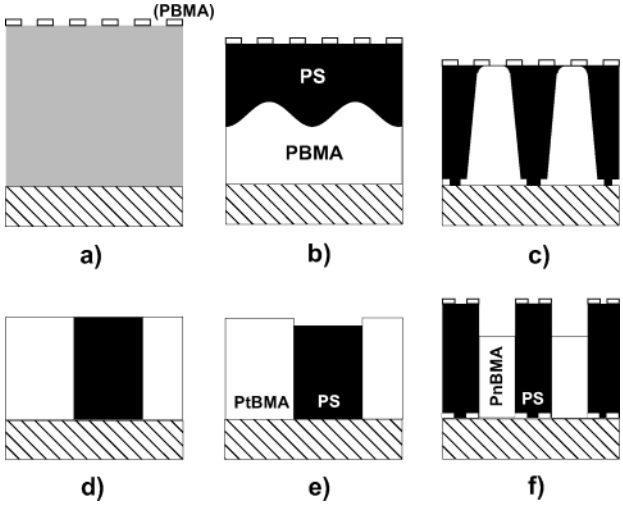

Figure 10. Schematic model describing morphology formation in PS film blends with PBMA isomers during spin-casting from toluene. Various stages correspond to (a) solvent-rich homogeneous (gray) fluid film with PBMA surface excess (white dashed line), (b) transient solution bilayer PS-rich (black)/ PBMA-rich (white) with developing interfacial instability, (c) breakup of the film and lateral domain arrangement (with PBMA excess at substrate), (d) quasi-2-dimensional coarsening of phase domains, and (e, f) surface topography reflecting frozen in place lateral domain structure. PS-rich domains are elevated (f) or slightly depressed (e) since PS solidifies earlier than PnBMA (f) but slightly later than PtBMA (e) (see T_g values in Table 1). Note that in reality the vertical extent of film structures presented in the figures is a few times lower that their horizontal dimensions.

c_S.[11,12,15] Third, the evolution of overall phase structure is terminated when c_S is so low that one of the homopolymers is no longer mobile.[15,20,30,68] The horizontal domain structure, although frozen in place, is reflected by surface topography (Figures 10c,f and 10d,e) since the rate of solidification due to solvent evaporation as well as polymer swelling in the remaining solvent is different for both polymer-rich phases.[15,30,69]

Surface Segregation. We postulate that phase separation and evolution during spin-casting are preceded (in one-phase region) by surface segregation in PBMA (Figure 10a), i.e., in a blend component with lower surface tension γ (see Table 1). We expect the spin-casting process to be very similar for both blend series (film thickness is almost constant, see section 3.1) but the phase evolution to proceed longer quench path for PS/PtBMA, which is more incompatible than PS/PnBMA.[65−67] Therefore, it is for PS/PtBMA that the PBMA molecules enriched (due to segregation) in subsurface regions (Figure 10a) are collected more effectively by horizontally coarsening (phase-separated) PBMA-rich domains. As a result, surface concentration Φ^S is here reduced and does not differ much from bulk composition Φ (in contrast to PS/PnBMA, see Figure 6). The additional (for PS/PtBMA, Figure 10c,d), regime of quasi-2-dimensional phase evolution explains also the observed systematic increase in the size $|S|^{1/2}$ of individual surface features (see Figure 4b).

Bilayer Formation. dSIMS data (section 3.3) indicate the PnBMA enrichment in film regions adjacent to the substrate. We interpret this excess as a vestige of PBMA-rich lamella of the transient bilayer domain structure[15,18,23,32] (substrate/ PBMA solution/ PS solution), formed at the onset of phase separation (Figure 10b). Such self-stratified lamellar structures were observed for other spin-cast blend films.[68,70] In turn, no distinct substrate excess in PBMA was observed in PS/PtBMA films. This is related as above (for diminished surface excess) with additional horizontal phase coarsening for this blend type. Two mechanisms can lead to the formation of transient substrate/PBMA solution/PS solution structure: First, more polar PBMA[52] can preferentially adsorb to (high-energy) polar SiO_x substrate[71] (a similar situation can be advocated for Au[15]). Second, lower solubility of one homopolymer can lead to its quicker depletion from the solvent and earlier solidification as a lamella onto the substrate.[18,19] Available values of solubility parameter δ (Table 1, confirmed by recent experimental results[69]) indicate this scenario to be plausible.

Instability Breaking Up Lamellar Structure. The compositional dependence of film topography (Figures 2 and 3) reveals two regions of droplet-type morphology (dominated by holes or islands) separated by bicontinuous structures at PnBMA [PtBMA] composition $\Phi_{i-h} \sim 0.65(4)$ [0.75(4)], different from the critical value $\Phi_C = 0.52$ [0.50]. The horizontal domain structure, reflected by film topography, cannot therefore be explained here by bulk phase coarsening confined into two dimensions.[20] This evolution mechanism (Figure 10c,d) can only supplement the breakup[32] of the lamellar structure necessary to reduce unfavorable PS/PBMA interfaces (their horizontal dimensions are in the film a few times larger than their vertical extent). The breakup can result from interfacial (capillary, dewetting)[15,18,19,32] or hydrodynamic (convective)[30,36,37,42] instability. While the latter seems to be less plausible[32] here (as the films of pure blend components show no surface undulations, Figures 2a,i and 3a,i), the former is indicated by several observations, made (mainly) for the hole-dominated structures of PS/PnBMA films: First, the holes recorded at low PBMA compositions Φ are accompanied by elongated ribbonlike structures of weak surface undulations (Figure 2b,c), resembling patterns formed at early stages of spinodal interfacial (dewetting) instability.[46]

Second, while the holes grow in size with PBMA content Φ (Figure 2) they are much less distinct[26] or not resolved[24] in films (with $\Phi \leq 0.40$) much thinner than used in this study. This suggests that the parameter of importance is here the thickness of the PBMA-rich solvent layer (Figure 10b). Hence, the relevant mechanism involves destabilization of this layer related with interfacial instability[43−45] of the interface PBMA solution/ PS solution (Figure 10b,c).

Long-range van der Waals interactions can be efficient as forces destabilizing multilayer structures over distances up to at least 125 nm[45] (an even higher range was suggested recently by dewetting phenomenon concluded for spin-cast polymer blend films[19]). Such long-range interactions between medium 1 and 3 across the layer 2 (PBMA) contribute to its excess free energy (per unit area) $\Delta G_2 = -A_{123}/(12\pi h_2^2)$. The layer is unstable, when the effective Hamaker constant A_{123}[72] is positive.[45,46] Positive and negative sign of the constant A_{123} is evaluated[73] for the multilayer structure substrate (SiO_x)/PBMA/PS and air/PBMA/PS, respectively. This is in accord with the transient lamellar arrangement (substrate/PBMA solution/PS solution) suggested by experimental data.

Scaling Test for Interfacial Instability. For thermodynamically unstable PBMA-rich lamella, small thermal fluctuations of the PBMA/PS interface grow spontaneously, leading to spinodal decomposition[43,46] of the PBMA (solution) layer. Factors governing the related kinetics in such a multilayer structure are not known.[45] However, on the basis of earlier evaluations for dewetting liquid layer on a solid[43] and a liquid[44] substrate, we could expect that spontaneous undulations are characterized by the wavelength λ_u proportional to the square of layer thickness ($\lambda_u \sim h_2^2$). An early stage of spinodal layer decomposition is reflected in the bicontinuous pattern of interface undulations[46] developed into isolated droplets of size proportional to λ_u.[43] Both morphology features are reflected by free surface topography (Figures 2b,c, 2b−e, and 3b−e). We assume that the thickness h_2 is proportional to PBMA blend composition Φ and individual droplet size λ_u to the square root of average area $|S|^{1/2}$ of individual dominant surface feature. To test the scaling law $\lambda_u \sim h_2^2$,[43,44] the relation $|S|^{1/4}$ vs Φ is plotted in Figure 4b for both blend types. Two data sets, corresponding to droplet-type morphologies ($\Phi < \Phi_{i-h}$) in PS/PnBMA and PS/PtBMA films, are both well described by a linear relation. The regression to the PS/PnBMA data points (circles in Figure 4b) approaches the origin, indicating that the destabilization of the PBMA-rich layer is here the main phase evolution process and suggesting that the assumptions made (on complete phase separation into bilayers and the relation between phase structure and surface topography) are reasonable. The linear relation for the PS/PtBMA data (triangles in Figure 4b) is shifted to higher $|S|^{1/4}$ values, indicating an additional period of horizontal phase coarsening. While the above-described phase evolution mechanism was verified using the data corresponding to blend composition $\Phi < \Phi_{i-h}$, we believe that it is also relevant for other PBMA concentrations (when droplets merge and the analytical approach used is not valid), similarly to suggestions made for another system studied recently.[18]

Surface Topography Reflecting Lateral Domain Structure. The second stage of spin-casting ends with overall lateral phase domain arrangement frozen in place. During the third stage free surface undulations are formed due to solvent evaporation, reflecting horizontal film structure. The relevant mechanism[30] relates earlier solidification of the domains rich in polymer A (as compared with the phase rich in polymer B) with higher glass transition temperature $T_g(A) > T_g(B)$.[74] The A-rich regions turn solid, when domains rich in B are still swollen. Finally, because of further solvent evaporation, B-rich domains collapse. As a result, the regions rich in A are elevated in the frozen surface topography. This simple model[15,30,69] explains vertical arrangement of blend phases and even (qualitatively) the vertical extent Δh of formed surface patterns (Figures 10c,f and 10d,e): For the PS/PnBMA pair, the glass point of PS is much higher (by $\Delta T_g = 80$ deg) than that of PnBMA. PS-rich domains are always elevated, and the vertical extent Δh of surface patterns can reach even ∼60 nm. Surface topographies are dominated by PnBMA-rich[75] holes for $\Phi < \Phi_{i-h}$ (high PS composition) and by PS-rich islands for $\Phi > \Phi_{i-h}$ (low PS composition, Figure 2). In turn, for the PS/PtBMA pair, it is PS that has lower glass transition ($\Delta T_g = 22$ deg, smaller than for the other couple). Here PS-rich domains form always slightly lower surface areas and the vertical extent $\Delta h \sim 18$ nm is here smaller. Surface patterns are dominated by PtBMA-rich[75] islands for $\Phi < \Phi_{i-h}$ (high PS composition) and by PS-rich holes for$\Phi > \Phi_{i-h}$ (low PS composition, Figure 3).

5. Summary and Conclusions

Structure formation in spin-cast polymer blend films cannot be observed directly, and therefore its mechanisms are usually concluded based on examination of structures formed in systems with modified parameters, for instance exchanged solvents, substrates, and/or polymers.[11,13,15,17] This approach was applied here to the polymer mixtures with exchanged isomers (PS/PnBMA and PS/PtBMA). The postulated morphology formation stages involve surface segregation in PBMA, rise of transient bilayer, interfacial instability of PBMA lamella and horizontal phase rearrangement, and reproduction of lateral domain structure by surface topography. The branching of butyl methacrylate (Figure 1) increases both immiscibility with PS[67] and glass transition temperature T_g.[52] These two *microstructural features* affect structure formation: The first one introduces additional (for PS/PtBMA) horizontal phase coarsening regime, which reduces PBMA excess at the surface and substrate and increases lateral domain size. The second feature speeds up solidification of PBMA-rich phase as compared to PS-rich domains, yielding elevated PtBMA surface regions in contrast to depressed PnBMA areas. Last but not least, this work presents also a *quantitative test* (Figure 4b) for the compositional scaling ($|S|^{1/2} \propto \Phi^2$) of the average size of individual dominant surface features (reflecting dropletlike domains), expected for *interfacial (capillary) instability* (of transient layer with thickness $\propto \Phi$)[43,44] taking place in the course of spin-casting.

Acknowledgment. This work was partially supported by the Reserve of the Rector of the Jagellonian University and the Polish Committee for Scientific Research (mainly Grant 1P03B1027). We thank Prof. M. Szymoński for the access to AFM apparatus.

References and Notes

(1) Sirringhaus, H.; Kawase, T.; Friend, R. H.; Shimoda, T.; Inbasekaran, M.; Wu, W.; Woo, E. P. *Science* **2000**, *290*, 5499.

(2) Snaith, H. J.; Arrias, A. C.; Morteani, A. C.; Silva, C.; Friend, R. H. *Nano Lett.* **2002**, *2*, 1353.
(3) Moons, E. *J. Phys.: Condens. Matter* **2002**, *14*, 12235.
(4) Walheim, S.; Schäffer, E.; Mlynek, J.; Steiner, U. *Science* **1999**, *283*, 520.
(5) Urbas, A.; Sharp, R.; Fink, Y.; Thomas, E. L.; Xenidou, M.; Fetters, L. J. *Adv. Mater.* **2000**, *12*, 812.
(6) Haupt, M.; Miller, S.; Ladenburger, A.; Sauer, R.; Thonke, K.; Spatz, J. P.; Riethmüller, S.; Möller, M.; Banhart, F. *J. Appl. Phys.* **2002**, *91*, 6057.
(7) Krausch, G. *Mater. Sci. Eng.* **1995**, *R14*, 1.
(8) Binder, K. *Adv. Polym. Sci.* **1999**, *138*, 1.
(9) Budkowski, A. *Adv. Polym. Sci.* **1999**, *148*, 1.
(10) Geoghegan, M.; Krausch, G. *Prog. Polym. Sci.* **2003**, *28*, 261.
(11) Gutmann, J. S.; Müller-Buschbaum, P.; Stamm, M. *Faraday Discuss.* **1999**, *112*, 258.
(12) Budkowski, A.; Bernasik, A.; Cyganik, P.; Rysz, J.; Brenn, R. *e-Polym.* **2002**, *006*, 1.
(13) Tanaka, K.; Takahara, A.; Kajiyama, T. *Macromolecules* **1996**, *29*, 3232.
(14) Affrossman, S.; Henn, G.; O'Neill, S. A.; Pethrick, R. A.; Stamm, M. *Macromolecules* **1996**, *29*, 5010.
(15) Walheim, S.; Böltau, M.; Mlynek, J.; Krausch, G.; Steiner, U. *Macromolecules* **1997**, *30*, 4995.
(16) Böltau, M.; Walheim, S.; Mlynek, J.; Krausch, G.; Steiner, U. *Nature (London)* **1998**, *391*, 877.
(17) Affrossman, S.; O'Neill, S. A.; Stamm, M. *Macromolecules* **1998**, *31*, 6280.
(18) Ton-That, C.; Shard, A. G.; Teare, D. O. H.; Bradley, R. H. *Polymer* **2001**, *42*, 1121.
(19) Ton-That, C.; Shard, A. G.; Bradley, R. H. *Polymer* **2002**, *43*, 4973.
(20) Dalnoki-Veress, K.; Forrest, J. A.; Stevens, J. R.; Dutcher, J. R. *J. Polym. Sci., Part B: Polym. Phys.* **1996**, *34*, 3017.
(21) Dalnoki-Veress, K.; Forrest, J. A.; Stevens, J. R.; Dutcher, J. R. *Physica A* **1997**, *239*, 87.
(22) Walheim, S.; Ramstein, M.; Steiner, U. *Langmuir* **1999**, *15*, 4828.
(23) Müller-Buschbaum, P.; Gutmann, J. S.; Stamm, M. *Macromolecules* **2000**, *33*, 4886.
(24) Affrossman, S.; Jerome, R.; O'Neill, S. A.; Schmitt, T.; Stamm, M. *Colloid Polym. Sci.* **2000**, *278*, 993.
(25) Gutmann, J. S.; Müller-Buschbaum, P.; Schubert, D. W.; Stribeck, N.; Stamm, M. *J. Macromol. Sci., Phys. B* **1999**, *38*, 563.
(26) Chen, C.; Wang, J.; Woodcock, S. E.; Chen, Z. *Langmuir* **2002**, *18*, 1302.
(27) Cyganik, P.; Bernasik, A.; Budkowski, A.; Bergues, B.; Kowalski, K.; Rysz, J.; Lekki, J.; Lekka, M.; Postawa, Z. *Vacuum* **2001**, *63*, 307.
(28) Cyganik, P.; Budkowski, A.; Raczkowska, J.; Postawa, Z. *Surf. Sci.* **2002**, *507*−*510*, 700.
(29) Raczkowska, J.; Rysz, J.; Budkowski, A.; Lekki, J.; Lekka, M.; Bernasik, A.; Kowalski, K.; Czuba, P. *Macromolecules* **2003**, *36*, 2419.
(30) Budkowski, A.; Bernasik, A.; Cyganik, P.; Raczkowska, J.; Penc, B.; Bergues, B.; Kowalski, K.; Rysz, J.; Janik, J. *Macromolecules* **2003**, *36*, 4060.
(31) Cyganik, P.; Budkowski, A.; Steiner, U.; Rysz, J.; Bernasik, A.; Walheim, S.; Postawa, Z.; Raczkowska, J. *Europhys. Lett.* **2003**, *62*, 855.
(32) Sprenger, M.; Walheim, S.; Budkowski, A.; Steiner, U. *Interface Sci.* **2003**, *11*, 225.
(33) Hopkinson, I.; Myatt, M. *Macromolecules* **2002**, *35*, 5153.
(34) Lawrence, C. J. *Phys. Fluids* **1988**, *31*, 2786.
(35) Schubert, D. W. *Polym. Bull. (Berlin)* **1997**, *38*, 177.
(36) Mitov, Z.; Kumacheva, E. *Phys. Rev. Lett.* **1998**, *81*, 3427.
(37) de Gennes, P. G. *Eur. Phys. J. E* **2001**, *6*, 421.
(38) Hopkinson, I.; Kiff, F. T.; Richards, R. W.; King, S. M.; Munro, H. *Polymer* **1994**, *35*, 1722.
(39) Steiner, U.; Klein, J.; Eiser, E.; Budkowski, A.; Fetters, L. J. *Science* **1992**, *258*, 1126.
(40) Graessley, W. W.; Krishnamoorti, R.; Reichart, G. C.; Balsara, N. P.; Fetters, L. J.; Lohse, D. J. *Macromolecules* **1995**, *28*, 1260.
(41) Tretinnikov, O. N.; Otha, K. *Langmuir* **1998**, *14*, 915.
(42) Kumacheva, E.; Li, L.; Winnik, M. A.; Shinozaki, D. M.; Cheng, P. C. *Langmuir* **1997**, *13*, 2483.
(43) Brochard-Wyart, F.; Daillant, J. *Can. J. Phys.* **1990**, *68*, 1084.
(44) Brochard-Wyart, F.; Martin, P.; Redon, C. *Langmuir* **1993**, *9*, 3682.
(45) David, M. O.; Reiter, G.; Sitthai, T.; Schultz, J. *Langmuir* **1998**, *14*, 5667.
(46) Seemann, R.; Herminghaus, S.; Jacobs, K. *J. Phys.: Condens. Matter* **2001**, *13*, 4925 and references therein.
(47) Michielsen, K.; De Raedt, H. *Phys. Rep.* **2001**, *347*, 461.
(48) Mecke, K. R. *Phys. Rev. E* **1996**, *53*, 4794.
(49) Mecke, K. R. *Int. J. Mod. Phys. B* **1998**, *9*, 861.
(50) Michielsen, K.; De Raedt, H. *Comput. Phys. Commun.* **2000**, *132*, 94.
(51) Mecke, K. R. *Fluid Phase Equilib.* **1998**, *150*, 591.
(52) Brandrup, J.; Immergut, E. H.; Grulke, E. A. *Polymer Handbook*, 4th ed.; J. Wiley & Sons: New York, 1999.
(53) Frank, C. W.; Gashgari, M. A. *Macromolecules* **1979**, *12*, 163.
(54) Van Krevelen, D. W. *Properties of Polymers: Their Correlation with Chemical Structure*; Elsevier: New York, 1976.
(55) Choi, H.-Y.; Lee, D.-Y.; Lee, J.-Y.; Kim, J.-H. *J. Appl. Polym. Sci.* **2000**, *78*, 639.
(56) Gaonkar, A. G.; Neuman, R. D. *Colloids Surf.* **1987**, *27*, 1.
(57) Lekki, J.; Lekka, M.; Romano, H.; Cleff, B.; Stachura, Z. *Acta Phys. Pol., A* **1996**, *89*, 315.
(58) Rysz, J.; Ermer, H.; Budkowski, A.; Bernasik, A.; Lekki, J.; Juengst, G.; Brenn, R.; Kowalski, K.; Camra, J.; Lekka, M.; Jedliński, J. *Eur. Phys. J. E* **2001**, *5*, 207.
(59) Rysz, J.; Ermer, H.; Budkowski, A.; Lekka, M.; Bernasik, A.; Wróbel, S.; Brenn, R.; Lekki; J.; Jedliński, J. *Vacuum* **1999**, *54*, 303.
(60) Briggs, D. *Surface Analysis of Polymers by XPS and Static SIMS*, 1st ed.; Cambridge University Press: Cambridge, 1998.
(61) Bernasik, A.; Rysz, J.; Budkowski, A.; Kowalski, K.; Camra, J.; Jedliński, J. *Macromol. Rapid Commun.* **2001**, *22*, 829.
(62) For blend ($\Phi = 0.10$ and 0.90) films with asymmetric monomodal *h*-distribution the measures (Δh, F, χ_E) are determined as described in ref 29.
(63) Youngblood, J. P.; McCarthy, T. J. *Thin Solid Films* **2001**, *382*, 95.
(64) Ton-That, C.; Shard, A. G.; Bradley, R. H. *Langmuir* **2000**, *16*, 2281.
(65) Schubert, D. W.; Abetz, V.; Stamm, M.; Hack, T.; Siol, W. *Macromolecules* **1995**, *28*, 2519.
(66) Fischer, H.; Weidisch, R.; Stamm, M.; Budde, H.; Höring, S. *Colloid Polym. Sci.* **2000**, *278*, 1019.
(67) Kim, J. H.; Park, D. S.; Kim, C. K. *J. Polym. Sci., Part B: Polym. Phys.* **2000**, *38*, 2666.
(68) Geoghegan, M.; Jones, R. A. L.; Payne, R. S.; Sakellariou, P.; Clough, A. S.; Penfold, J. *Polymer* **1994**, *10*, 2019.
(69) Elbs, H.; Funkunaga, K.; Stadler, R.; Sauer, G.; Magerle, R.; Krausch, G. *Macromolecules* **1999**, *32*, 1204.
(70) Bernasik, A.; Włodarczyk-Miśkiewicz, J.; Łużny, W.; Kowalski, K.; Raczkowska, J.; Rysz, J.; Budkowski, A. *Synth. Met.* **2004**, *144*, 253.
(71) Fasolka, M. J.; Harris, D. J.; Mayes, A. M.; Yoon, M.; Mochrie, S. G. J. *Phys. Rev. Lett.* **1997**, *79*, 3018.
(72) Evans, D. F.; Wennerström, H. *The Colloidal Domain: Where Physics, Chemistry, Biology and Technology Meet*, 1st ed.; Wiley-VCH: New York, 1994.
(73) The effective Hamaker constant A_{123} for the interactions between medium 1 and 3 across layer 2, $A_{123} = (A_{11}^{1/2} - A_{22}^{1/2})(A_{33}^{1/2} - A_{22}^{1/2})$, $A_{ii} \sim$ surface tension γ_i,[72] and hence $A_{PBMA/PBMA} < A_{PS/PS}$ (see Table 1) in addition to $A_{air/air} = 0$ and $A_{PS/PS} \sim A_{SiO_x/SiO_x}$.[72] Therefore, $A_{air/PBMA/PS} < 0 < A_{SiO_x/PBMA/PS}$.
(74) While different solubility of PS and PBMA could in principle lead to (additional) solubility-induced swelling modification[15] this effect is less important here.
(75) A careful inspection of Figure 4a reveals that for low PBMA content this phase, present mainly in well defined dropletlike domains (holes for PS/PnBMA, islands for PS/PtBMA), is additionally distributed elsewhere (e.g., in vertical arrangements—remnants of early stage of interfacial instability in PS/PnBMA layers with $\Phi = 0.30$ and 0.40).

MA035815H